A MACROSCOPIC FINITE ELEMENT FOR A SYMMETRIC DOUBLE LAP JOINT SUBJECTED TO MECHANICAL AND THERMAL LOADING

Peter A. Gustafson, Anthony M. Waas
Department of Aerospace Engineering
University of Michigan, Ann Arbor, MI 48109, USA

Abstract

A thermo-mechanical analytical model and a corresponding macroscopic bonded joint finite element are presented for the analysis of orthotropic double lap joints subjected to combined thermal-mechanical loads. The analytical solution offers an improvement in accuracy over its predecessor[1, 2], at the cost of increased solution complexity. However, to facilitate the use of this solution, it has been incorporated into a macroscopic bonded joint finite element[3]. The single element reproduces the analytical solution with minimal analyst input, and therefore can be easily incorporated into early design studies. The macroscopic element provides a computationally efficient and mesh independent comparative stress result. To validate the element, the stress predictions of the single element are compared with a continuum finite element model. The current article is a summary of recent work[4].

1 Introduction

Advances in structural epoxies and adhesives have expanded the temperature range over which high performance fibrous composite materials can be used. In the structures composed of these materials, adhesively bonded joints are widely used due to improved load distribution, increased service life, reduced machining cost, and/or reduced complexity[5]. These epoxies and adhesives, designed to provide structural integrity at high temperature, are subjected to severe operating environments. Furthermore, manufacturing processes subject these materials to broad temperature ranges during the different stages of the curing cycle. It is known that high stress gradients can exist near the edges of bonded joints due to mismatches in thermal expansion coefficients and elastic moduli[6]. Therefore, components made from these materials carry a significant risk of adverse stress caused by differential thermal expansion, even when used at room temperature. Due to the increased use of composite materials and bonded joints, the need for efficient and effective thermo-mechanical analysis tools is greater than ever.

The design and modeling of bonded joints is not yet a mature field. Continuum finite element (FE) models of adhesively bonded joints are widely available in the literature, where work began as early as 1971 (Wooley and Garver[7], and Adams and Peppiatt[8] are early references). More recently, promising advances in cohesive zone (including Kafkalidis and Thouless[9], Xie et al.[10], Li et al.[11, 12], Valoroso and Champaney[13]), discrete cohesive zone (Xie et al.[14]), fracture mechanics (Weerts and Kossira[15]), probabilistic prediction (Aydemir and Gunay[16], Koutsourelakis et al.[17]), virtual crack closure (including Gillespie et al.[18], Wang et al.[19], Glaessgen et al.[20], Krueger [21], Xie et al.[22, 23, 24]), and other adhesive region models (including Munoz et al.[25], Goncalves et al.[26], Goyal et al.[27]) have greatly increased the predictive capability of FE techniques. Cohesive zone models have been incorporated into commercial software, including Abaqus®[28], as well as freely available research codes like Tahoe®[29]. However, despite their availability, the listed techniques are expensive and require user expertise. Therefore there are ongoing efforts to develop rapid analysis techniques (Oterkus et al.[30, 31], Smeltzer and Lundgren[32]), a key enabling technology for vehicle designers.

Though models built with the tools listed

above can be accurate and very capable, they rely on the presence of a meshed joint, where continuum elements represent the adherends, and the adhesive is represented by continuum elements or a discrete traction separation law. There is significant overhead in creating and analyzing joints using these and other continuum numerical methods. Mesh generation and manipulation is an obstacle for all but academic geometries. Mesh density is also a consideration, since the computational time for basic joints can be significant if non-linear material properties and material degradation criterion are included. As a result, there are ongoing efforts to evaluate analysis techniques that are less mesh dependent. For example, the Composites Affordability Initiative has recommended a p-based analysis code for analysis of adhesively bonded joints.[1] Use of p-based codes should be less mesh dependent than the more commonly used h-based FE codes. Similarly, Bednarcyk et al.[33] used a higher order, semi-analytical theory (developed for functionally graded materials) to analyze a double lap and a bonded doubler joint. This technique was reported to be less mesh dependent than h-based analysis methodologies.

Although the techniques cited above attempt to minimize mesh dependency, they do not eliminate it. Due to mesh generation overhead and computational cost, it is often impractical and sometimes impossible to include joint models in sub-system, system, or vehicle level models. In these instances, an appropriate single finite element representation of a joint could provide adequate representation of a joint's behavior in the structure being modeled. Such a joint element was suggested in Gustafson and Waas[3], and referred to as a Macroscopic Bonded Joint Finite Element (MBJFE). In concept, it was shown to provide basic joint performance analysis using a very limited number of degrees of freedom. The element's shape functions had a thermo-mechanical, orthotropic, lap-shear type analytical solution embedded within them. The internal displacement (strain) field of the element provided an adequate approximation of the field in a joint. Therefore, it predicted the stress response without significant meshing overhead. The MBJFE was intended to lay a foundation for advances in application specific joint elements for initial sizing in FE models at all system levels.

This article is an abbreviated presentation of the work described in Gustafson and Waas[4]. It is intended to disseminate that work for additional scrutiny.

2 Derivation of the advanced shear and peel model

In Gustafson et al.[2], a dimensionless solution was presented for a symmetric, orthotropic double lap joint subjected to thermo-mechanical loading. The lap joint is schematically represented in figure 1.1. The central adherend is referred to as material a, the outer adherend is referred to as material c. Material b is the adhesive, which is thin in comparison to the adherends. The objective is to determine the equilibrium stress response to thermal and mechanical loading. The material is assumed to be linear elastic and orthotropic, with linear orthotropic thermal expansion. The joint is assumed to deform in plane strain.

Examining a general parallelepiped as shown in figure 1.2, force equilibrium in x and y directions can be written as:

$$\begin{aligned}\sum F_1 &= \delta y\left(\sigma_{11}(x+\delta x,y)-\sigma_{11}(x,y)\right)\\ &\quad+\delta x\left(\tau_{12}(x,y+\delta y)-\tau_{12}(x,y)\right)\\ &=0\\ \sum F_2 &= \delta x\left(\sigma_{22}(x,y+\delta y)-\sigma_{22}(x,y)\right)\\ &\quad+\delta y\left(\tau_{12}(x+\delta x,y)-\tau_{12}(x,y)\right)\\ &=0,\end{aligned} \tag{1}$$

which can be rewritten as the shear-normal stress relationship for each constituent:

$$\begin{aligned}\frac{\partial\sigma_{11}(x,y)}{\partial x} &= -\frac{\partial\tau_{12}(x,y)}{\partial y}\\ \frac{\partial\sigma_{22}(x,y)}{\partial y} &= -\frac{\partial\tau_{12}(x,y)}{\partial x}.\end{aligned} \tag{2}$$

Several additional assumptions are made to ease the solution. The longitudinal normal stress in the adhesive is assumed to be zero, therefore Eqs. 2 dictates that the shear stress in the adhesive is a function of x only.[2] For convenience, the remaining shear stress fields are assumed to vary linearly in y throughout the specimen, therefore Eqs. 2 dictate that the adherend longitudinal normal stresses are also functions of x only, and that the peel stresses are linear functions of x and y.

[1] http://www.esrd.com [cited Feb. 2007]

[2] The limitations imposed by this assumption are described in Gustafson et al.[2].

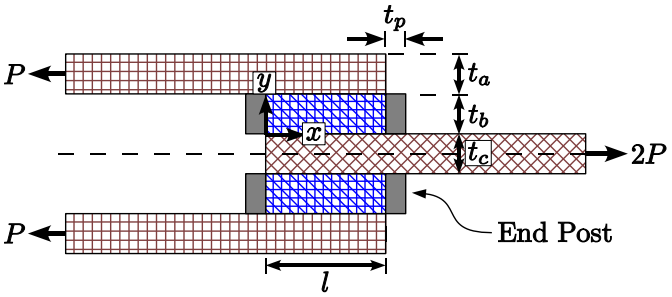

1.1: Schematic of the double lap joint with end posts

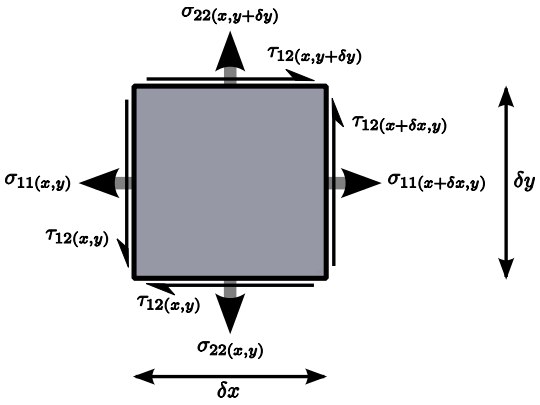

1.2: Generalized equilibrium parallelepiped

Traction free boundaries are present on the top and bottom surfaces. The centerline of the central adherend is free of shear due to symmetry. These requirements are expressed as:

$$\begin{aligned} \tau_{c12(x,t_b+t_c)} &= 0, \\ \sigma_{c22(x,t_b+t_c)} &= 0, \\ \tau_{a12(x,-\frac{t_a}{2})} &= 0. \end{aligned} \tag{3}$$

Stress continuity at the joint interfaces requires the following:

$$\begin{aligned} \sigma_{b22(x,0)} &= \sigma_{a22(x,0)}, \\ \sigma_{c22(x,tb)} &= \sigma_{b22(x,tb)}, \\ \tau_{b12(x,0)} &= \tau_{a12(x,0)}, \\ \tau_{c12(x,tb)} &= \tau_{b12(x,tb)}. \end{aligned} \tag{4}$$

Finally, longitudinal normal stress boundary conditions are imposed by the mechanical loads at the edges of central adherend a, and are expressed as:

$$\begin{aligned} \sigma_{a11(0)} &= 0, \\ \sigma_{a11(l)} &= \frac{2P}{t_a}, \end{aligned} \tag{5}$$

By sequentially writing a linear form for each stress component (using the stress field character described above), and by applying boundary and continuity conditions to determine the linear constants, equations can be written for each stress component in terms of the central adherend stress $\sigma_{a11}(x)$. The process is as described in Ref. [2] and is the same in this work, with the addition of several stress components ($\tau_{a12}(x,y)$, $\sigma_{a22}(x,y)$, $\tau_{c12}(x,y)$, $\sigma_{c22}(x,y)$). The resulting stress equations are detailed on the left side of table 1.

In addition to the boundary conditions specified in Eqs. 3, Eqs. 4, and Eqs. 5, the adhesive edge shear stress is forced to zero using the end post technique described in Gustafson et al.[2], which was inspired by the double lap joint solution of Davies[34]. The stresses in the edge posts also listed on the left side of table 1.

The solution for the central adherend normal stress ($\sigma_{a11}(x)$) is carried out by application of the principle of virtual forces, as described in detail in [4]. In summary, for each stress component (each is a function of $\sigma_{a11}(x)$), a corresponding virtual stress component is written in terms of the virtual normal stress $\hat{\sigma}_{a11}(x)$. These virtual stress components are shown on the right side of table 1. By integrating potential energy over the volume of the joint and minimizing for any admissible $\hat{\sigma}_{a11}(x)$, the central adherend stress field $\sigma_{a11}(x)$ is determined as a function of all material properties and loads. Subsequent grouping of all material terms according to their order of derivative (defined as β and γ in Eq. 6) and the loads according to thermal and mechanical contributions of the total load (defined as ϕ_T and ϕ_P respectively in Eq. 6), the differential equation can be written as:

$$\frac{\partial^4 \sigma_{a11}(x)}{\partial x^4} + \beta \frac{\partial^2 \sigma_{a11}(x)}{\partial x^2} + \gamma \sigma_{a11}(x) + \phi_T + \phi_P = 0. \tag{6}$$

Eq. 6 is identical in form to the solution given in [2], however the material constants β and γ, as well as the load constants ϕ_T and ϕ_P are more complex due to the increase in the retained stress components in the potential energy minimization. The improved accuracy of this model over its predecessor is a direct result of the addition of these previously neglected terms.

With an equation for the central adherend stress ($\sigma_{a11}(x)$), all stress components can easily

Table 1: Double lap joint stresses and virtual stresses expressed as functions of $\sigma_{a11}(x)$

Equilibrium Normal Stress	Virtual Normal Stress
$\sigma_{a11}(x)$	$\hat{\sigma}_{a11}(x)$
$\sigma_{c11}(x) = \frac{P}{t_c} - \frac{t_a\,\sigma_{a11}(x)}{2\,t_c}$	$\hat{\sigma}_{c11}(x,y) = -\frac{t_a\,\hat{\sigma}_{a11}(x)}{2\,t_c}$
$\sigma_{a22}(x,y) = \frac{d^2}{dx^2}\sigma_{a11}(x)\left(\frac{y^2+t_a y}{2} - \frac{t_a(t_c+2t_b)}{4}\right)$	$\hat{\sigma}_{a22}(x,y) = \frac{d^2}{dx^2}\hat{\sigma}_{a11}(x)\left(\frac{y^2+t_a y}{2} - \frac{t_a(t_c+2t_b)}{4}\right)$
$\sigma_{b22}(x,y) = \frac{t_a\left(\frac{d^2}{dx^2}\sigma_{a11}(x)\right)(2y-t_c-2t_b)}{4}$	$\hat{\sigma}_{b22}(x,y) = \frac{t_a\left(\frac{d^2}{dx^2}\hat{\sigma}_{a11}(x)\right)(2y-t_c-2t_b)}{4}$
$\sigma_{c22}(x,y) = -\frac{t_a\left(\frac{d^2}{dx^2}\sigma_{a11}(x)\right)(y-t_c-t_b)^2}{4t_c}$	$\hat{\sigma}_{c22}(x,y) = -\frac{t_a\left(\frac{d^2}{dx^2}\hat{\sigma}_{a11}(x)\right)(y-t_c-t_b)^2}{4t_c}$
Equilibrium Shear Stress	**Virtual Shear Stress**
$\tau_{a12}(x,y) = -\frac{\frac{d}{dx}\sigma_{a11}(x)(2y+t_a)}{2}$	$\hat{\tau}_{a12}(x,y) = -\frac{\frac{d}{dx}\hat{\sigma}_{a11}(x)(2y+t_a)}{2}$
$\tau_{b12}(x) = -\frac{t_a\left(\frac{d}{dx}\sigma_{a11}(x)\right)}{2}$	$\hat{\tau}_{b12}(x,y) = -\frac{t_a\left(\frac{d}{dx}\hat{\sigma}_{a11}(x)\right)}{2}$
$\tau_{c12}(x,y) = \frac{t_a\left(\frac{d}{dx}\sigma_{a11}(x)\right)(y-t_c-t_b)}{2t_c}$	$\hat{\tau}_{c12}(x,y) = \frac{t_a\left(\frac{d}{dx}\hat{\sigma}_{a11}(x)\right)(y-t_c-t_b)}{2t_c}$
Equilibrium End Post Stress	**Virtual End Post Stress**
$\sigma_{p22}(\bar{x}=0,y) = \frac{t_a\left(\frac{d}{d\,x}\,\sigma_{a11}(x)\right)(y-t_b)}{2\,t_p}$	$\hat{\sigma}_{p22}(\bar{x}=0,y) = \frac{t_a\left(\frac{d}{d\,x}\,\hat{\sigma}_{a11}(x)\right)(y-t_b)}{2\,t_p}$
$\sigma_{p22}(\bar{x}=1,y) = -\frac{t_a\left(\frac{d}{d\,x}\,\sigma_{a11}(x)\right)(y-t_b)}{2\,t_p}$	$\hat{\sigma}_{p22}(\bar{x}=1,y) = -\frac{t_a\left(\frac{d}{d\,x}\,\hat{\sigma}_{a11}(x)\right)(y-t_b)}{2\,t_p}$

be determined using the equations in table 1. It was noted in Ref. [2] that non-dimensionalization and load normalization of (6) is possible, and doing so provides a mechanism for separation of the responses to mechanical and thermal loads. As described in Ref. [3], this has great benefits for the MBJFE solution when used with an iterative solver. Therefore, without explicitly reporting the dimensional material and load constants (β, γ, ϕ_T, ϕ_P), non-dimensionalization and load normalization is done so as to conform to the solution provided in Ref. [2]. The dimensionless and load normalized material, load, and stress terms are defined as follows:

$$\begin{aligned}
\bar{x} &= \tfrac{x}{l}, & \bar{\beta} &= l^2\beta,\\
\bar{\gamma} &= l^4\gamma, & \bar{\phi}_T &= \phi_T\tfrac{l^4}{E_{a11}},\\
\bar{\phi}_P &= \phi_P\tfrac{l^4}{E_{a11}}, & \bar{\bar{\phi}}_{total} &= \bar{\phi}_P + \bar{\phi}_T,\\
\bar{\bar{\phi}}_P &= \tfrac{\bar{\phi}_P}{\bar{\bar{\phi}}_{total}}, & \bar{\bar{\sigma}}_{\kappa ij(\bar{x})} &= \tfrac{\sigma_{\kappa ij(l\bar{x})}}{E_{a11}\bar{\bar{\phi}}_{total}}.
\end{aligned} \tag{7}$$

In Eq. 7, $\bar{x}$ is the dimensionless spatial coordinate measured from the left edge of the joint, $\bar{\beta}$ and $\bar{\gamma}$ are dimensionless material parameters, and $\bar{\phi}_P$ and $\bar{\phi}_T$ are the dimensionless mechanical and thermal loads respectively. A dimensionless total load is defined as $\bar{\bar{\phi}}_{total}$, which is used to further normalize the stresses $\bar{\bar{\sigma}}_{\kappa ij(\bar{x})}$. Similarly, a mechanical fraction of the dimensionless total load is defined as $\bar{\bar{\phi}}_P$. Each of the terms in Eq. 7 are explicitly defined according to the constitutive and load quantities in [4]. Now, Eq. 8 from Ref. [2] is written as the form most suitable for the MBJFE:

$$\begin{aligned}
\bar{\bar{\sigma}}_{a11}\left(\bar{x},\bar{\bar{\phi}}_P\right) = &+\bar{\bar{A}}\left(\bar{\bar{\phi}}_P\right)e^{\bar{\lambda}_1\bar{x}} + \bar{\bar{B}}\left(\bar{\bar{\phi}}_P\right)e^{-\bar{\lambda}_1\bar{x}}\\
&+\bar{\bar{C}}\left(\bar{\bar{\phi}}_P\right)e^{\bar{\lambda}_3\bar{x}} + \bar{\bar{D}}\left(\bar{\bar{\phi}}_P\right)e^{-\bar{\lambda}_3\bar{x}} - \frac{1}{\gamma}.
\end{aligned} \tag{8}$$

In Eq. 8, the material parameters are recast in the form of the roots of the bi-quadratic differential equation.

$$\bar{\lambda}^2_{[13]} = \frac{-\bar{\beta} \pm \sqrt{\bar{\beta}^2 - 4\bar{\gamma}}}{2}. \tag{9}$$

The equations for the dimensionless basis coefficients ($\bar{\bar{A}}\left(\bar{\bar{\phi}}_P\right)$, $\bar{\bar{B}}\left(\bar{\bar{\phi}}_P\right)$, $\bar{\bar{C}}\left(\bar{\bar{\phi}}_P\right)$, $\bar{\bar{D}}\left(\bar{\bar{\phi}}_P\right)$) are identical to those given in Ref. [2] and are listed below:

$$\begin{aligned}
\bar{\bar{A}}\left(\bar{\bar{\phi}}_P\right) &= \frac{\mu_3\mu_{A_P}}{\mu_1\mu_2}\bar{\bar{\phi}}_P + \frac{\mu_{A_T}}{\mu_1},\\
\bar{\bar{B}}\left(\bar{\bar{\phi}}_P\right) &= \frac{\mu_3\mu_{B_P}}{\mu_1\mu_2}\bar{\bar{\phi}}_P + \frac{\mu_{B_T}}{\mu_1},\\
\bar{\bar{C}}\left(\bar{\bar{\phi}}_P\right) &= \frac{\mu_3\mu_{C_P}}{\mu_1\mu_2}\bar{\bar{\phi}}_P + \frac{\mu_{C_T}}{\mu_1},\\
\bar{\bar{D}}\left(\bar{\bar{\phi}}_P\right) &= \frac{\mu_3\mu_{D_P}}{\mu_1\mu_2}\bar{\bar{\phi}}_P + \frac{\mu_{D_T}}{\mu_1},
\end{aligned} \tag{10}$$

In Eq. 10, the coefficients ($\bar{\bar{A}}\left(\bar{\bar{\phi}}_P\right)$, $\bar{\bar{B}}\left(\bar{\bar{\phi}}_P\right)$, $\bar{\bar{C}}\left(\bar{\bar{\phi}}_P\right)$, $\bar{\bar{D}}\left(\bar{\bar{\phi}}_P\right)$) are linear functions of the mechanical fraction of the total load ($\bar{\bar{\phi}}_P$) and several

variables denoted by μ which are combinations of the material parameters. These are given in the [4]. In combination, Eq. 8 and Eq. 10 effectively separate the thermal and mechanical responses.

It is recognized that the presented solution in this section would be incomplete without additional information provided in Ref. [2], particularly with respect to the application of boundary conditions which bridge between the differential equation (Eq. 6) and the stress solution (Eq. 8). Further, Ref. [2] provides complete detail regarding the load normalized form of Eq. 8.

3 Formulation of the finite element

Figure 1 schematically shows the MBJFE originally derived in Gustafson and Waas[3]. The element is a 1D element, with all displacement degrees of freedom being oriented along the 1-axis. Two of the displacement degrees of freedom, q_1 and q_4, are external degrees of freedom which connect the joint element to the external structure. The remaining displacement degrees of freedom are internal to the element, and are used in conjunction with Lagrange multipliers to determine the mechanical loading fraction, $\bar{\bar{\phi}}_P$, required for determination of the stress and strain fields governed by Eq. 8. The mechanical load that is carried across the joint is calculated using internal degrees of freedom, P_1 and P_2 .

The element in figure 1 is composed of three subelements. The outer subelements span q_1 - q_2, and q_3 - q_4. These subelements are essentially truss elements, and their principal purpose is to establish the mechanical load as an internal degree of freedom as described in Ref. [3], where their contribution to the element stiffness is given in detail. The joint section subelement spans q_2 - q_3, and is responsible for predicting the relevant joint stresses as well as correctly representing the stiffness of the joint. The form of the stiffness matrix was developed in Ref. [3]. To update the subelement to the more accurate stress functions developed above, the displacement interpolation (shape functions) must be updated, as is detailed in subsection 3.1.

3.1 Stiffness and Load Contribution of the Adhesively Bonded Section

The subelement stiffness matrix is directly dependent on the load-displacement response of the central and outer adherends. The strain in these adherends is related, via the material constitutive response, to the stress fields known from Eq. 8 and table 1. These strains are related to the stiffness matrix by shape functions derivatives, and this relationship was given in Ref. [3] as Eq. 11.

$$K_e = \frac{\sum_{\kappa} E_{\kappa 11} \int_{y_{\kappa 0}}^{y_{\kappa 1}} \int_0^1 B_\kappa^2 \left(\bar{x}, \bar{\bar{\phi}}_P\right) d\bar{x}\, dy_\kappa}{l_e} \begin{bmatrix} 1 & -1 \\ -1 & 1 \end{bmatrix} \tag{11}$$

In the discrete space of the FE model, the known or desired quantities are the applied temperature change (ΔT, assumed to be constant through the element) and the nodal loads and displacements. The load quantities must be recast into their non-dimensional forms to conform to the stress equations given above. Non-dimensionalizing constants ($\frac{\Theta}{\theta_{\Delta T}}$ and $\frac{\Theta}{\theta_P}$) are defined so that:

$$\begin{aligned} \Delta T &= \frac{\Theta}{\theta_{\Delta T}} \bar{\phi}_T, \\ P &= \frac{\Theta}{\theta_P} \bar{\phi}_P. \end{aligned} \tag{12}$$

Application of Eqs. 12 to the known stress field and constitutive law, the strain can be written as a linear function of the total load $\bar{\bar{\phi}}_{total}$:

$$\begin{aligned} \frac{\varepsilon_{a11}}{\bar{\bar{\phi}}_{total}} =& (1 - \nu_{a13}\nu_{a31}) \cdot \\ & \left[+e^{-\bar{\lambda}_3 \bar{x}} \bar{\bar{D}} \left(\bar{\bar{\phi}}_P\right) + e^{\bar{\lambda}_3 \bar{x}} \bar{\bar{C}} \left(\bar{\bar{\phi}}_P\right) \right. \\ & \left. + e^{-\bar{\lambda}_1 \bar{x}} \bar{\bar{B}} \left(\bar{\bar{\phi}}_P\right) + e^{\bar{\lambda}_1 \bar{x}} \bar{\bar{A}} \left(\bar{\bar{\phi}}_P\right) - \frac{1}{\bar{\gamma}} \right] \\ & + \frac{\Theta}{\theta_{\Delta T}} \left(1 - \bar{\bar{\phi}}_P\right) \left(\alpha_{a33}\nu_{a31} + \alpha_{a11}\right), \\ \frac{\varepsilon_{c11}}{\bar{\bar{\phi}}_{total}} =& \frac{E_{a11} t_a \left(\nu_{c13}\nu_{c31} - 1\right)}{2 E_{c11} t_c} \cdot \\ & \left[+e^{-\bar{\lambda}_3 \bar{x}} \bar{\bar{D}} \left(\bar{\bar{\phi}}_P\right) + e^{\bar{\lambda}_3 \bar{x}} \bar{\bar{C}} \left(\bar{\bar{\phi}}_P\right) \right. \\ & \left. + e^{-\bar{\lambda}_1 \bar{x}} \bar{\bar{B}} \left(\bar{\bar{\phi}}_P\right) + e^{\bar{\lambda}_1 \bar{x}} \bar{\bar{A}} \left(\bar{\bar{\phi}}_P\right) \right] \\ & + \frac{\Theta}{\theta_{\Delta T}} \left(1 - \bar{\bar{\phi}}_P\right) \left(\alpha_{c11} + \alpha_{c33}\nu_{c31}\right) \\ & + \frac{1}{E_{c11} t_c} \left(1 - \nu_{c13}\nu_{c31}\right) \left(\frac{E_{a11} t_a}{2\bar{\gamma}} + \frac{\bar{\bar{\phi}}_P \frac{\Theta}{\theta_P}}{1} \right). \end{aligned} \tag{13}$$

It is assumed that the total elongation is the same for the adherends, therefore the two elongation equations are written as:

$$\begin{aligned} q_e &= \left(\frac{dx}{d\bar{x}}\right) \int_0^1 \varepsilon_{a11} \left(\bar{x}, \bar{\bar{\phi}}_P, \bar{\bar{\phi}}_{total}\right) d\bar{x}, \\ q_e &= \left(\frac{dx}{d\bar{x}}\right) \int_0^1 \varepsilon_{c11} \left(\bar{x}, y, \bar{\bar{\phi}}_P, \bar{\bar{\phi}}_{total}\right) d\bar{x}, \end{aligned} \tag{14}$$

where the subelement elongation q_e is defined as:

$$q_e = q_4 - q_3. \tag{15}$$

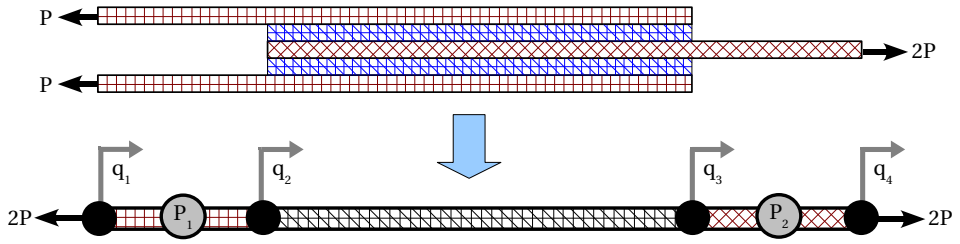

Figure 1: Symmetric double lap joint and MBJFE representation.

In Eq. 14, the elongation is written as a function of the non-dimensional total load, $\bar{\bar{\phi}}_{total}$. The total load is not known *a priori* and must be eliminated in favor of an available quantity (the total elongation q_e) so that a stiffness matrix can be calculated. This is accomplished by applying the boundary condition to the result of Eq. 14:

$$\begin{aligned}
\left(\frac{dx}{d\bar{x}}\right)\int_0^{\bar{x}} \varepsilon_{a11}\left(\bar{x},\bar{\bar{\phi}}_P,\bar{\bar{\phi}}_{total}\right)d\bar{x}\Big|_{\bar{x}=0} &= 0,\\
\left(\frac{dx}{d\bar{x}}\right)\int_0^{\bar{x}} \varepsilon_{a11}\left(\bar{x},\bar{\bar{\phi}}_P,\bar{\bar{\phi}}_{total}\right)d\bar{x}\Big|_{\bar{x}=1} &= q_e,\\
\left(\frac{dx}{d\bar{x}}\right)\int_0^{\bar{x}} \varepsilon_{c11}\left(\bar{x},\bar{\bar{\phi}}_P,\bar{\bar{\phi}}_{total}\right)d\bar{x}\Big|_{\bar{x}=0} &= 0,\\
\left(\frac{dx}{d\bar{x}}\right)\int_0^{\bar{x}} \varepsilon_{c11}\left(\bar{x},\bar{\bar{\phi}}_P,\bar{\bar{\phi}}_{total}\right)d\bar{x}\Big|_{\bar{x}=1} &= q_e,
\end{aligned} \tag{16}$$

Specifically, the elongation is zero when $\bar{x} = 0$ (since $\bar{x} = 0$ is the reference from which elongation is measured), and the total elongation is q_e when $\bar{x} = 1$. Applying these boundary conditions and solving for the total load $\bar{\bar{\phi}}_{total}$ as a function of elongation q_e (this is done for each strain equation), total load can be replaced in Eq. 13 with the following:

$$\begin{aligned}
\bar{\bar{\phi}}_{total_a} &= \bar{\bar{\Phi}}_a q_e,\\
\bar{\bar{\phi}}_{total_c} &= \bar{\bar{\Phi}}_c q_e,
\end{aligned} \tag{17}$$

where the constants ($\bar{\bar{\Phi}}_a$, $\bar{\bar{\Phi}}_c$) are detailed in [4]. Substituting Eq. 17 into Eq. 13, the displacement field is known in terms of total elongation and the shape functions and shape functions derivatives can now be written for each adherend:

$$\begin{aligned}
u_a\left(\bar{x},\bar{\bar{\phi}}_P,q_e\right) &= N_a\left(\bar{x},\bar{\bar{\phi}}_P\right)q_e,\\
u_c\left(\bar{x},\bar{\bar{\phi}}_P,q_e\right) &= N_c\left(\bar{x},\bar{\bar{\phi}}_P\right)q_e,\\
B_a\left(\bar{x},\bar{\bar{\phi}}_P\right) &= \frac{d}{d\bar{x}}N_a\left(\bar{x},\bar{\bar{\phi}}_P\right),\\
B_c\left(\bar{x},\bar{\bar{\phi}}_P\right) &= \frac{d}{d\bar{x}}N_c\left(\bar{x},\bar{\bar{\phi}}_P\right).
\end{aligned} \tag{18}$$

The complete shape functions in Eq. 18 are given in detail in [4].

Having established the appropriate shape functions, the stiffness matrix can now be integrated numerically using Eqs. 11. Additionally, the subelement load vector was derived in Ref. [3] as Eq. 19, and can now be calculated. In Eqs. 11 and Eq. 19, the summation includes both adherends ($\kappa = a, c$).

$$\vec{F} = \left[P + \sum_{\kappa}\alpha_{\kappa 11}\Delta T E_{\kappa 11}\int_{y_0}^{y_1}\int_0^1 B_\kappa\, d\bar{x}\, dy_\kappa\right]\left\{\begin{array}{c}-1\\1\end{array}\right\} \tag{19}$$

The final requirement for element calculations is knowledge of the mechanical load P, used to determine the load character $\bar{\bar{\phi}}_P$ of the bonded section sub-element. This is accomplished by causing this load to be an internal degree of freedom using Lagrange multipliers. In this work, the load becomes P_1. The complete description of this process is as presented in Ref. [1] and is not repeated here.

3.2 The Abaqus® Subroutine

The sub-element stiffness matrices and load vectors, developed above and in Ref. [3], are assembled into element matrices with 6 DOFs using a standard assembly technique[35]. The formulation requires an iterative solution, since the mechanical load carried by the joint is not known in general. Therefore, the shape functions developed above have been implemented as a user element subroutine (UEL) for the commercial nonlinear FE package Abaqus®[28]. A complete description of the UEL functionality is provided in Ref. [3], including the modified midpoint rule numerical integration technique.

The field quantities are calculated from table 1 at each integration point, based on the calculated

Table 2: Model size for ASTM double lap joints

Model	Nodes	Elements	DOFs
CPE4	~ 22100	~ 21600	~ 44300
UEL	4	1	6

ΔT and P_1 for the increment. The user specifies the number of integration points to be the number of stress prediction points desired in the joint. In this way, all stress and strain quantities of interest are calculated in a manner consistent with the shape function displacement field.

4 FE output

The stress prediction provided by the UEL has been compared to a plane strain continuum FE model. In the case of the UEL, the entire model consists of a single element. In the case of the continuum model, a 2D mesh has been generated. Both models are based on the ASTM International double lap joint[36]. An overview of the continuum mesh, as well as the assumed geometry, material properties, and loading are reported in [4]. The solver used is Abaqus® Standard, and the continuum mesh consists entirely of linear plain strain elements (CPE4). Half of the joint is modeled due to symmetry. The mechanical load is applied far away from the lap joint and the thermal load is applied to all nodes. Displacement symmetry constraints are enforced along the mid-plane of the central adherend. Non-linear geometric stiffness is assumed.

Aluminum (Al) is used as the central adherend in all models; the outer adherends are Titanium (Ti), and AS4/3501-6 (AS4)[37]. For simplicity, the adhesive properties are assumed to be isotropic, and are estimated base on Cytec FM300 adhesive. The shear stresses from the continuum model are reported at the centerline of the adhesive, which is the most representative location for comparison with the uniform shear stress predicted by the UEL. The peel stress in the continuum model is reported at the interface between the adhesive and the central adherend. The choice of this location has a large effect on the predicted peel stress as was reported in [4]. However, the adhesive to central adherend interface (a-b) comparison location is chosen because the UEL model can be used as a measure of the *magnitude* of the singularity present at this location. The peel stress reported from the UEL is the average peel stress through the thickness (the stress equation is evaluated at $y = \frac{t_b}{2}$).

4.1 Comparison of MBJFE and continuum based FE models

Plots of the stresses predicted by the continuum and UEL models are shown in figures 2 and 3. In each, the shear stress is shown in subfigures a,c, and e for thermal, mechanical, and mixed loading respectively. Similarly, the peal stress is shown in subfigures b,d, and f for thermal, mechanical, and mixed loading respectively.

In all cases of the Al-Ti joint, the peak shear stress predicted by the UEL matches the continuum model adequately (figures 2.1, 2.3 and 2.5). The peak location is consistently found to be further from the edge in the UEL than in the continuum model, owing to the form of the derived governing differential equation. The peel stress predicted by the UEL is in adequate agreement with the continuum model (figures 2.2, 2.4 and 2.6). Unlike the continuum model, the UEL predicted value does not suffer from any mesh dependency and is therefore well suited for use in joint-to-joint comparison. The stress predicted by the UEL is similar to the continuum model, and is representative of the unconverged singular peel stress result.

The UEL solution is orthotropic, and an example of a composite application is shown in figures 3. These figures show an Al-AS4 joint subjected to thermal, mechanical, and mixed loading, where the fibers are oriented longitudinally (0^o). The two figures shows that the UEL solution is in adequate agreement with the continuum solution for all three load types, demonstrating the effectiveness of the UEL in composite joints.

Based on the cumulative agreement shown in figures 2 and 3 as well as similar plots presented in [4], it can be concluded that the UEL element adequately predicts the shear stress in a double

lap joint. The peel stress predicted by the UEL model is found to be consistently in agreement with the *magnitude* of the (unconverged) singular stress field in all figures (at the mesh density used in this comparison). Therefore, it can be used as a mesh independent indicator of peel stress magnitude, useful for joint-to-joint comparison.

5 Conclusion

In this article, a Macroscopic Bonded Joint Finite Element has been described. It is capable of predicting the lap joint field quantities in the bonded zone while using only six degrees of freedom. It does so without burdening the user with mesh dependency or significant meshing overhead. The described MBJFE accomplishes this task by embedding an analytical solution directly within the element. Its stiffness and load response are based on non-linear shape functions that are dependent on the load character. All critical terms are formulated as functions of the dimensionless mechanical load fraction, $\bar{\bar{\phi}}_P$, allowing for solution via an iterative, non-linear FE solver. To demonstrate its capability, the element has been implemented as a user element subroutine in the commercial finite element package Abaqus®.

Based on comparison with a traditional FE solution, the MBJFE has been shown to be capable of adequately predicting stress and strain due to thermal and mechanical loads in a single, four noded element with six degrees of freedom. With this element, initial sizing and trade studies can be accomplished with a greatly reduced meshing investment, as well as a reduction in computation time, when compared with the standard finite element method. This work lays a firm foundation for further advancements in macroscopic joint elements. It is anticipated that currently available analytical solutions can be reformulated as application specific macroscopic joint elements.

Acknowledgments

This work was supported by the Space Vehicle Technology Institute under grant NCC3-989 jointly funded by NASA and the Department of Defense. It is managed within the NASA Constellation University Institutes Project, with Claudia Meyer as the project manager. P.A. Gustafson also extends gratitude to all contributors to the Maxima project, which was used for symbolic calculations.

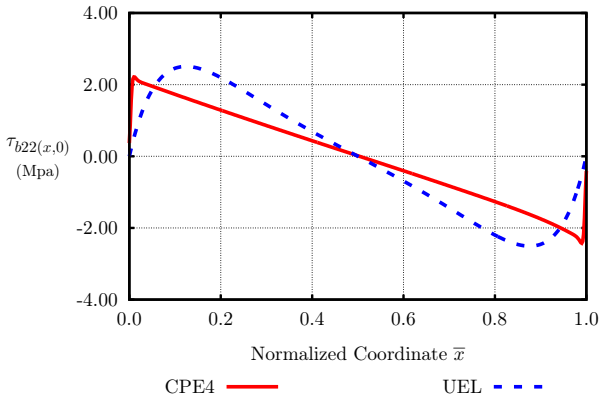

2.1: $\tau_{b12}(x)$ due to $\bar{\phi}_T$

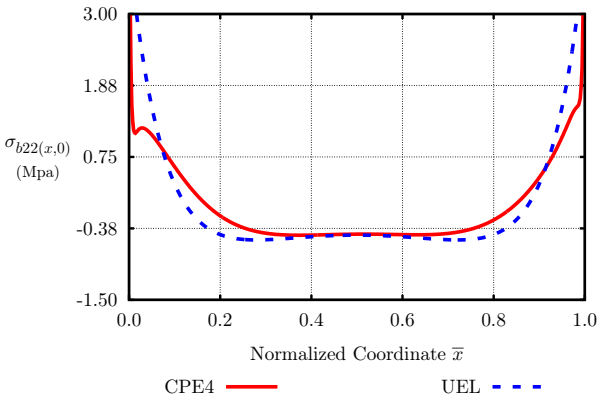

2.2: $\sigma_{b22}(x, y)$ due to $\bar{\phi}_T$

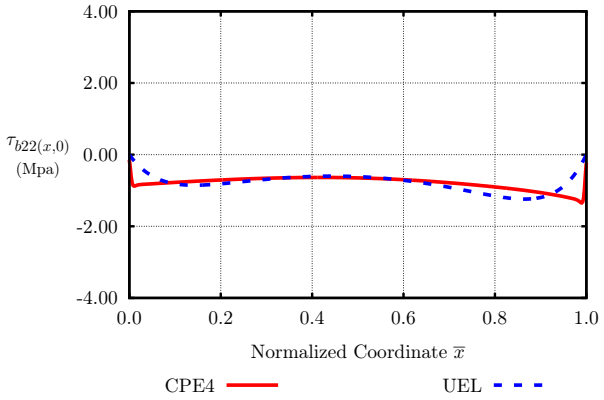

2.3: $\tau_{b12}(x)$ due to $\bar{\phi}_P$

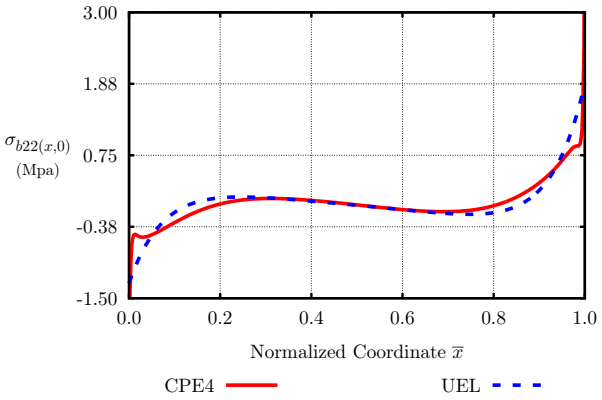

2.4: $\sigma_{b22}(x, y)$ due to $\bar{\phi}_P$

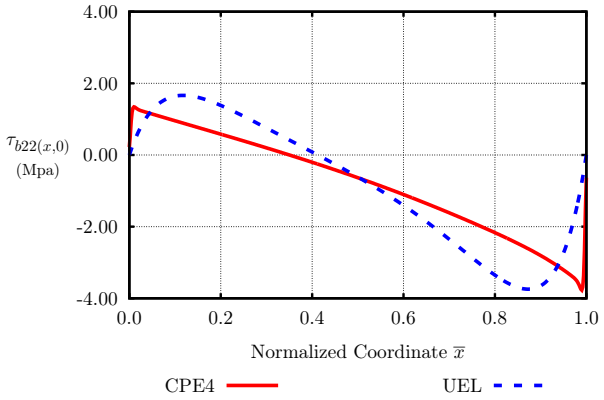

2.5: $\tau_{b12}(x)$ due to $\bar{\phi}_P + \bar{\phi}_T$

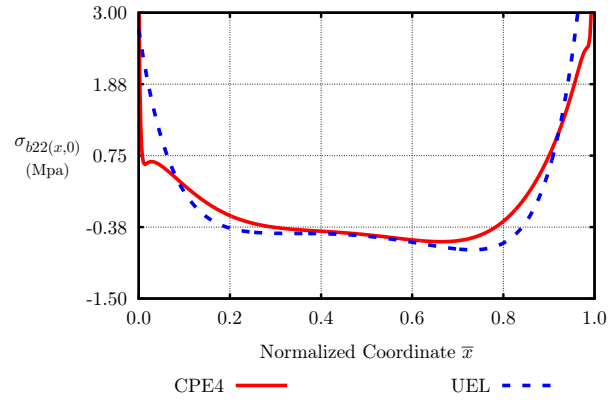

2.6: $\sigma_{b22}(x, y)$ due to $\bar{\phi}_P + \bar{\phi}_T$

Figure 2: Continuum and UEL models of Al-Ti joint

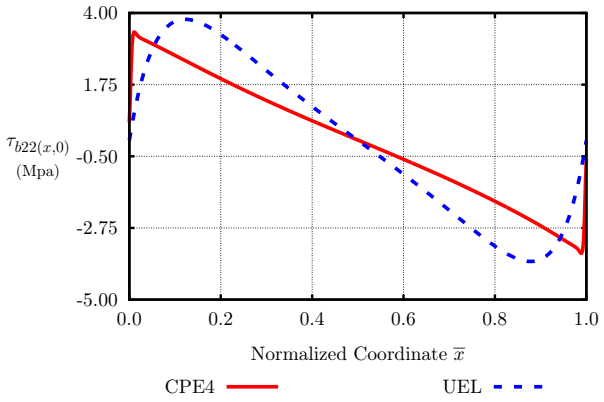

3.1: $\tau_{b12}(x)$ due to $\bar{\phi}_T$

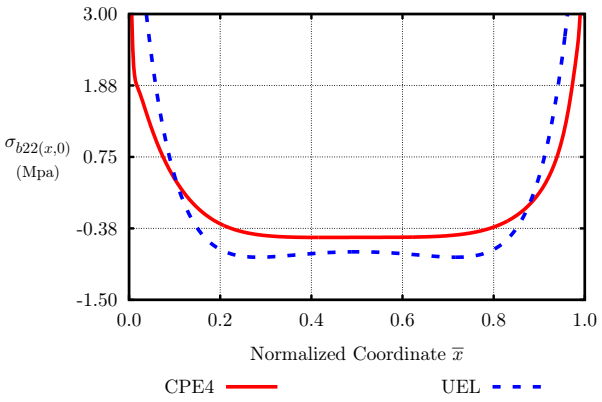

3.2: $\sigma_{b22}(x, y)$ due to $\bar{\phi}_T$

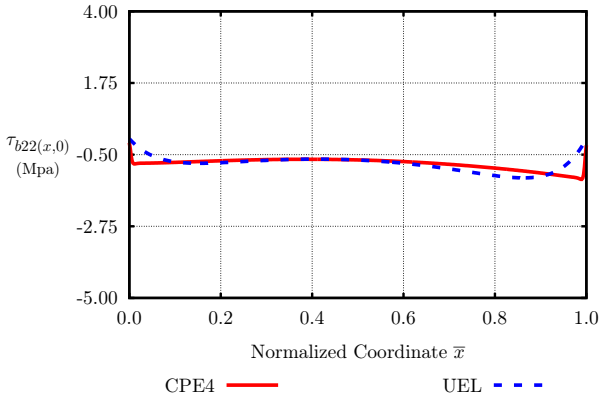

3.3: $\tau_{b12}(x)$ due to $\bar{\phi}_P$

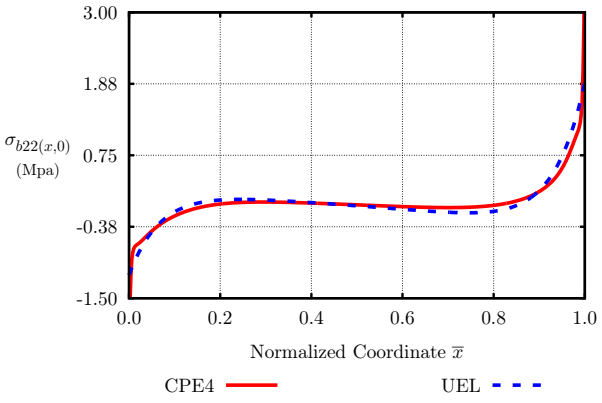

3.4: $\sigma_{b22}(x, y)$ due to $\bar{\phi}_P$

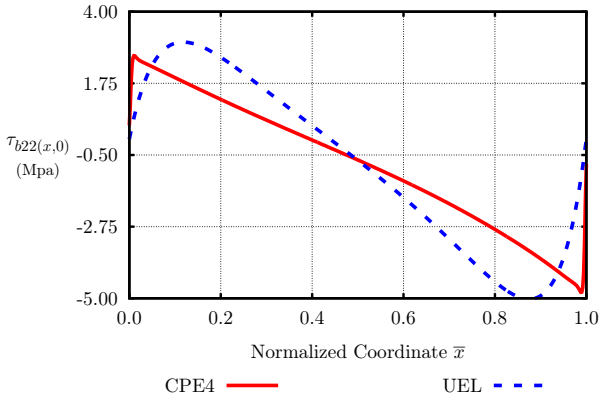

3.5: $\tau_{b12}(x)$ due to $\bar{\phi}_P + \bar{\phi}_T$

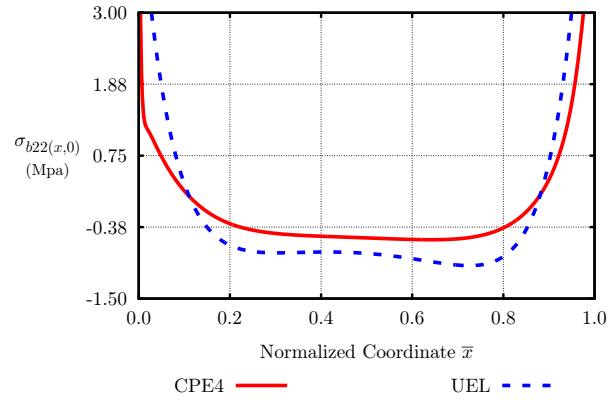

3.6: $\sigma_{b22}(x, y)$ due to $\bar{\phi}_P + \bar{\phi}_T$

Figure 3: Continuum and UEL models of Al-AS4 (0°) joint

References

[1] P. A. Gustafson, A. Bizard, and A. M. Waas, "Dimensionless parameters in symmetric double lap joints: an orthotropic solution for thermomechanical loading," in *Proceedings of the AIAA/ASME/ASCE/AHS/ASC 47th Structures, Structural Dynamics, and Materials Conference, May 1-4 2006, Newport RI*, no. 2006-1959, American Institute of Aeronautics and Astronautics, 2006.

[2] P. A. Gustafson, A. Bizard, and A. M. Waas, "Dimensionless parameters in symmetric double lap joints: An orthotropic solution for thermomechanical loading," *International Journal of Solids and Structures*, 2007 In Press.

[3] P. A. Gustafson and A. M. Waas, "A macroscopic joint finite element for a symmetric double lap joint," in *Proceedings of the American Society of Composites 21st Annual Technical Conference*, no. 204, American Society of Composites, Sept 2006.

[4] P. A. Gustafson and A. M. Waas, "A macroscopic finite element for a symmetric doublelap joint subjected to mechanical and thermal loading," in *Proceedings of the AIAA/ASME/ASCE/AHS/ASC 48th Structures, Structural Dynamics, and Materials Conference, Apr 23-26 2007, Honolulu HI*, no. 2007-2308, American Institute of Aeronautics and Astronautics, 2007.

[5] R. Adams, J. Comyn, and W. Wake, *Structural Adhesive Joints in Engineering*. Chapman and Hall, 1997.

[6] E. Oterkus, E. Madenci, S. Smeltzer III, and D. Ambur, "Thermomechanical analysis of bonded cylindrically curved composite shell structures," in *Proceedings of the AIAA/ASME/ASCE/AHS/ASC 47th Structures, Structural Dynamics, and Materials Conference, May 1-4, Newport, RI*, no. 2006-1963, American Institute of Aeronautics and Astronautics, 2006.

[7] G. R. Wooley and D. R. Carver, "Stress concentration factors for bonded lap joints," *J. Aircraft*, vol. 8, pp. 817–820, 1971.

[8] R. D. Adams and N. A. Peppiatt, "Stress analysis of adhesive-bonded lap joints," *J. Strain Analysis*, vol. 9, no. 3, pp. 185–196, 1974.

[9] M. S. Kafkalidis and M. D. Thouless, "The effects of geometry and material properties on the fracture of single lap-shear joints," *International Journal of Solids and Structures*, vol. 39, pp. 4367–4383, Aug. 2002.

[10] D. Xie, A. M. Waas, K. W. Shahwan, J. A. Schroeder, and R. G. Boeman, "Fracture criterion for kinking cracks in a tri-material adhesively bonded joint under mixed mode loading," *Engineering Fracture Mechanics*, vol. 72, pp. 2487–2504, Nov. 2005.

[11] S. Li, M. Thouless, A. Waas, J. Schroeder, and P. Zavattieri, "Use of a cohesive-zone model to analyze the fracture of a fiber-reinforced polymer-matrix composite," *Composites Science and Technology*, vol. 65, pp. 537–549, Mar. 2005.

[12] S. Li, M. Thouless, A. Waas, J. Schroeder, and P. Zavattieri, "Competing failure mechanisms in mixed-mode fracture of an adhesively bonded polymer-matrix composite," *International Journal of Adhesion and Adhesives*, vol. 26, pp. 609–616, Dec. 2006.

[13] N. Valoroso and L. Champaney, "A damage-mechanics-based approach for modelling decohesion in adhesively bonded assemblies," *Engineering Fracture Mechanics*, vol. In Press, Corrected Proof, pp. – , 2006.

[14] D. Xie and A. M. Waas, "Discrete cohesive zone model for mixed-mode fracture using finite element analysis," *Engineering Fracture Mechanics*, vol. 73, pp. 1783–1796, Sept. 2006.

[15] U. Weerts and H. Kossira, "Mixed mode fracture characterization of adhesive joints," in *ICAS Congress*, International Congress Aeronautical Sciences, 2000. Harrogate (GB), pp 451.1-451.9.

[16] A. Aydemir and D. Gunay, "The fuzzy finite element stress analysis of adhesive-bonded single lap joints," *Turkish J. Eng. Env. Sci*, pp. 121–127, 2003.

[17] P. Koutsourelakis, K. Kuntiyawichai, and G. Schueller, "Effect of material uncertainties on fatigue life calculations of aircraft fuselages: A cohesive element model," *Engineering Fracture Mechanics*, vol. 73, pp. 1202–1219, June 2006.

[18] J. W. Gillespie, Jr, L. A. Carlsson, and R. B. Pipes, "Finite element analysis of the end notched flexure specimen for measuring mode ii fracture toughness," *Composites Science and Technology*, vol. 27, no. 3, pp. 177–197, 1986.

[19] J. T. Wang, I. S. Raju, and D. W. Sleight, "Fracture mechanics analyses of composite skin-stiffener debond configurations with shell elements," No. 94-1389 -CP, 1994.

[20] E. Glaessgen, I. Raju, and J. C.C. Poe, "Fracture mechanics analysis of stitched stiffener-skin debonding," No. 98-2022, 1998.

[21] R. Krueger, "Virtual crack closure technique: History, approach, and applications," *Applied Mechanics Reviews*, vol. 57, no. 2, pp. 109–143, 2004.

[22] D. Xie, A. M. Waas, K. W. Shahwan, J. A. Schroeder, and R. G. Boeman, "Computation of energy release rates for kinking cracks based on virtual crack closure technique," *Computer Modeling in Engineering & Sciences*, vol. 6, pp. 515–524, 2004.

[23] D. Xie, A. G. Salvi, A. M. Waas, and A. Caliskan, "Discrete cohesive zone model to simulate static fracture in carbon fiber textile composites," in *46th AIAA/ASME/ASCE/AHS/ASC Structures, Structrual Dynamics and Materials Conference*, 2005.

[24] D. Xie and J. Sherrill B. Biggers, "Progressive crack growth analysis using interface element based on the virtual crack closure technique," *Finite Elem. Anal. Des.*, vol. 42, no. 11, pp. 977–984, 2006.

[25] J. Munoz, U. Galvanetto, and P. Robinson, "On the numerical simulation of fatigue driven delamination with interface elements," *International Journal of Fatigue*, vol. 28, pp. 1136–1146, Oct. 2006.

[26] J. P. M. Goncalves, M. F. S. F. de Moura, and P. M. S. T. de Castro, "A three-dimensional finite element model for stress analysis of adhesive joints," *International Journal of Adhesion and Adhesives*, vol. 22, no. 5, pp. 357–365, 2002.

[27] V. K. Goyal, E. R. Johnson, and C. Cassino, "Computational model for progressive failure of adhesivley bonded joints," in *44th AIAA/ASME/ASCE/AHS/ASC Structures, Structrual Dynamics and Materials Conference*, 2003.

[28] ABAQUS, Inc, *ABAQUS User Manual v6.5*. Electronic Version, 2006.

[29] Sandia National Laboratory, *Tahoe User Guide*, 3.4.1 ed., May 2003.

[30] E. Oterkus, A. Barut, E. Madenci, S. Smeltzer III, and D. Ambur, "Nonlinear analysis of bonded composite single-lap joints," in *Proceedings of the AIAA/ASME/ASCE/AHS/ASC 45th Structures, Structural Dynamics, and Materials Conference, April 19-22, Palm Springs, CA*, no. 2004-1560, American Institute of Aeronautics and Astronautics, 2004.

[31] E. Oterkus, E. Madenci, S. Smeltzer III, and D. Ambur, "Nonlinear analysis of bonded composite tubular lap joints," in *Proceedings of the AIAA/ASME/ASCE/AHS/ASC 46th Structures, Structural Dynamics, and Materials Conference, April 18-21, Austin, TX*, no. 2005-2380, American Institute of Aeronautics and Astronautics, 2005.

[32] S. S. Smeltzer III and E. Lundgren, "Analytical and numerical results for an adhesively bonded joint subjected to pure bending," in *Proceedings of the AIAA/ASME/ASCE/AHS/ASC 47th Structures, Structural Dynamics, and Materials Conference, May 1-4 2006, Newport RI*, no. 2006-1960, American Institute of Aeronautics and Astronautics, 2006.

[33] B. A. Bednarcyk, J. Zhang, C. S. Collier, Y. Bansal, and M. J. Pindera, "Analysis tools for adhesively bonded composite joints, part 1: Higher-order theory," *AIAA JOURNAL*, vol. 44, pp. 171–180, Jan. 2006.

[34] G. Davies, *Virtual work in structural analysis*. John Wiley & Sons, 1982.

[35] R. D. Cook, D. S. Malkus, and M. E. Plesha, *Concepts and applications of finite element analysis*. John Wiley & Sons, 1989.

[36] ASTM International, *ASTM D 3528-96 Standard Test Method for Strength Properties of Double Lap Shear Adhesive Joints by Tension Loading*.

[37] C. T. Herakovich, *Mechanics of fibrous composites*. John Wiley and Sons, Inc, 1998.